Published in final edited form as:
Anal Chem. 2011 February 1; 83(3): 888–895. doi:10.1021/ac102566f.

Silicon Field Effect Transistors as Dual-Use Sensor-Heater Hybrids

Bobby Reddy Jr[1,2,*], **Oguz H. Elibol**[4,5,*,&], **Pradeep R. Nair**[4,5], **Brian R. Dorvel**[1], **Felice Butler**[4,6], **Zahab Ahsan**[1], **Donald E. Bergstrom**[4,6], **Muhammad A. Alam**[4,5], and **Rashid Bashir**[1,2,3,*]

[1] Micro and Nano Technology Laboratory, University of Illinois at Urbana-Champaign, Urbana, IL 61801

[2] Department of Electrical and Computer Engineering, University of Illinois at Urbana-Champaign, Urbana, IL 61801

[3] Department of Bioengineering, University of Illinois at Urbana-Champaign, Urbana, IL 61801

[4] Birck Nanotechnology Center, Purdue University, West Lafayette, IN 47907

[5] School of Electrical and Computer Engineering, Purdue University, West Lafayette, IN 47907

[6] Department of Medicinal Chemistry and Molecular Pharmacology, Purdue University, West Lafayette, IN 47907

Abstract

We demonstrate the temperature mediated applications of a previously proposed novel localized dielectric heating method on the surface of dual purpose silicon field effect transistor (FET) sensor-heaters and perform modeling and characterization of the underlying mechanisms. The FETs are first shown to operate as electrical sensors via sensitivity to changes in pH in ionic fluids. The same devices are then demonstrated as highly localized heaters via investigation of experimental heating profiles and comparison to simulation results. These results offer further insight into the heating mechanism and help determine the spatial resolution of the technique. Two important biosensor platform applications spanning different temperature ranges are then demonstrated: a localized heat-mediated DNA exchange reaction and a method for dense selective functionalization of probe molecules via the heat catalyzed complete desorption and reattachment of chemical functionalization to the transistor surfaces. Our results show that the use of silicon transistors can be extended beyond electrical switching and field-effect sensing to performing localized temperature controlled chemical reactions on the transistor itself.

Introduction

Silicon field-effect transistors have found many applications, including their prolific use as the fundamental building block of electronics[1], their capability as chemical sensors[2], and

Corresponding Author: Rashid Bashir, rbashir@illinois.edu, Mailing Address: 2000 Micro and Nanotechnology Laboratory, MC-249, University of Illinois at Urbana-Champaign, 208 North Wright Street, Urbana, IL 61801, Phone: (217) 333-3097, Fax: (217) 244-6375.
*Authors have contributed equally
&Now at Intel Corporation, Santa Clara, CA.

Supporting Information Available
The supporting information for this work includes two figures that were referenced in this manuscript, including simulation profiles showing that dielectric relaxation of the ions is the primary mechanism for heating, simulation results showing the effect of scaling down device width, and control results from the heating and refunctionalization experiments.

their more recent uses as ultra-sensitive, label-free biological sensors with targets ranging from DNA or protein assays to early cancer diagnosis[3–4]. These sensing elements are potentially envisioned as integrated components for lab-on-a-chip applications. Because nearly all bio-chemical reactions are highly temperature dependent, these lab-on-a-chip devices often require precise control of temperature profiles in fluid. A localized, precise heating element capable of the heating of fluids in the picoliter to microliter range would be important for a variety of applications including DNA amplification by polymerase chain reaction (PCR)[5], patterning of distinct protein probes with high spatial resolution[6], localized cell lysis via heat[7], investigation of reaction kinetics, localized biochemical reactions, and temperature enhanced molecular synthesis.

Most currently reported heating techniques have focused on conduction based heating, using such devices as resistive heaters in close proximity to the heated area[8–9], Peltier elements[10], or Joule heating with electroosmotic flow[11]. Typically, these techniques require a large heated surface or element that is in close proximity to the areas to be heated. This results in large volumes of fluid being heated, which can limit the achievable spatial resolution of the applications. In addition, the fabrication processes for these elements are usually highly specialized, which is not amenable to integration with other lab-on-a-chip components. Microwave dielectric heating can be preferable to such methods because it is a non-contact method of heating using microwave energy that is delivered directly to the intended fluidic environment with little interference from the substrate[12]. In this case, ions in the fluid itself are used to increase the temperature only where electric fields are present, allowing for much higher spatial resolution. Furthermore, because microwave heating does not rely on thermal diffusion, heat can be applied with much higher thermocycling rates and reduced reaction times[13]. Much work has been reported using microwave heating for many applications[14–16], but these cases either use macroscale microwaves that will be difficult to scale down to on chip devices, or demonstrate low spatial resolution even with complicated microfluidics or waveguiding for enhancement.

We recently reported a technique for the use of silicon based field effect biosensors as localized microwave heating elements capable of heating fluid with high spatial resolution within a few nanometers of the insulator surface of the devices[17]. These dual use devices could potentially remove the need for separate components on chip by combining two critical needs of lab-on-a-chip devices – localized heaters and label free sensors – into a single element. In addition, the top down fabrication process employing standard CMOS techniques can be easily integrated with other essential components, such as control electronics. The broad applications for such a heating technique, which introduces a new dimension to the standard transistor sensing element, could extend from ultra-localized biochemical reactions on chip to densely packed integrated sensors targeted at the simultaneous detection of many distinct analytes. In this paper, we first demonstrate that these previously presented devices can be used as pH sensors in fluid. We then further investigate the heating technique by using device cross sections and experimentally observed heating profiles to optimize numerical simulation results to quantitatively determine the achievable spatial resolution of the technique in both the lateral and vertical directions. Next, we present two such applications as proofs of concept. We performed a temperature-mediated exchange reaction performed on the silicon transistor surface with high spatial confinement. This application demonstrates the first steps towards elaborate biochemical reactions on chip, such as local polymerase chain reaction (PCR) systems on chip with integrated sensing[5]. We also demonstrate a method for the self aligned patterning of distinct probes on two sensing elements in close proximity to one another. The precise patterning of a selective functional layer with nanoscale spatial resolution in a self aligned fashion is critical for the realization of sensitive and dense arrays of biosensors. Significant progress has been made towards this front but techniques reported to-date are not self-

aligned[18–22], lack high spatial resolution[23], are limited to specific chemistries on conductive surfaces only[24–25] with unknown reliability[26], or are limited in their operational environment[8]. A versatile, self-aligned and high-spatial resolution technique is needed.

Materials and Methods

Device Fabrication

The fabrication flow and preparation of devices, as well as techniques for heating and imaging were presented previously[17]. Briefly, a top-down fabrication was used, starting with Silicon on Insulator (SOI) wafers. The top silicon was thinned down to approximately 300 Å via dry oxidation and buffered oxide etch, the active area was lithographically defined, and the top silicon was etched using Deep Reactive Ion Etch (DRIE). After source and drain doping, a gate oxide of around 300 Å was grown, and metal contacts (200 Å titanium/800 Å platinum) to the FET devices were defined via liftoff. As part of this step, an on chip platinum fluid gate electrode was defined, which is important for fluidic measurements. A Plasma Enhanced Chemical Vapor Deposited (PECVD) oxide was deposited over the entire surface as a passivation layer to reduce leakage currents during fluid measurements (Figure 1a). The passivation layer in the area directly over the sensor regions was then removed using a dilute BOE etch, resulting in the cross section shown in Figure 1b. Final devices were 300 Å thick, 2 μm in width, and 10 μm in length.

Electrical Measurements and pH Sensing

The electrical configuration for both electrical measurements (sensor) and temperature mediated applications (heater) are shown in Figure 2a. Electrical contact to the devices was made via probing with micromanipulators. Back gate contact was achieved using a conductive chuck in contact with the backside substrate of the chips. Fluid gate contact was made using the on-chip platinum fluid gate electrode mentioned previously. All current measurements and applied biases were controlled by a semiconductor parameter analyzer (Kiethley 4200). Sodium phosphate buffers (10 mM) were used as pH solutions. The solution was confined to the area over the sensors using a custom made well constructed of polydimethylsiloxane (PDMS). The color plots shown in Figure 2c were generated by measuring the source drain current (I_{DS}) while sweeping the back gate voltage (V_{BG}) and stepping the fluid gate voltage (V_{FG}).

Surface Functionalization

Unless otherwise noted, all chemicals were purchased from Sigma-Aldrich and were used without further purification. Peptide nucleic acid (PNA) was purchased from and purified via high performance liquid chromatography (HPLC, >95%) by Applied Biosystems. PNA was characterized by mass spectroscopy; theoretical: (m/z) 2961.90, observed: (m/z) 2961.2. Locked nucleic acid (LNA) was purchased from and purified via HPLC by Sigma-Proligo. LNA was characterized by MALDI-MS; LNA6-BHQ theoretical: (m/z) 2622, observed: (m/z) 2542; LNA8 theoretical: (m/z) 2662, observed: (m/z) 2660. All DNA was purchased from and purified via HPLC by Sigma Genosys, a part of Sigma Aldrich. All fluorophore and amine modifications were performed by Sigma Genosys as well. A list of all molecules used in the experiments is shown in Table 1.

DNA Attachment

Chips were cleaned with a Piranha solution (H_2O_2:H_2SO_4)(3:1), rinsed with DI water, then dried using a stream of nitrogen immediately before the start of the chemistry. Subsequent steps were performed in a glove box purged with high purity nitrogen.

Samples were silanized in a 3% 3-aminopropyltrimethoxysilane (purchased from Sigma-Aldrich) in a methanol:DI(19:1) solution for 30 minutes at room temperature. Subsequently, the samples were rinsed with methanol and DI water, and dried with nitrogen. Later, chips were cured using a hot plate at 110° C for 5 minutes. Chips were placed into a *N*,*N*-dimethylformamide (DMF) solution containing 10% pyridine and 1 mM 1,4-phenylene diisothiocyanate (PDITC) for 2 hours for surface activation. Chips were then rinsed with DMF and 1,2-dichloroethane and dried with nitrogen. The chips were then inserted in a solution of amine-modified probe DNA at a 1 μM concentration in a 1.0 M tris-HCl [pH 7.0] with 1 % vol/vol *N*,*N*-diisopropylethylamine and 20 % vol/vol dimethylsulfoxide (DMSO) buffer, and allowed to incubate overnight. Later, chips were rinsed with methanol and DI water and dried with nitrogen. In order to prevent non-specific adsorption, the remaining un-reacted PDITC were deactivated by immersing the chip in 50 mM 6-amino-1-hexanol and 150 mM *N*,*N*-diisopropylethylamine in DMF for a minimum of 2 hours. Chips were then rinsed with DMF, methanol and DI water and dried with nitrogen.

Individual devices were heated in 10^{-2}×TBE (Tris-borate EDTA) buffer solution (pH 7.5, ionic strength: 0.09 mM) by using the setup outlined in the electrical setup for heating section. Typically an AC voltage of 10 MHz at 18 V_{rms} for 5 minutes was applied to the back gate for the removal of the molecules unless otherwise specified.

PNA Attachment and Exchange Reaction Procedures

Lysine modified FAM-PNA8 molecules were immobilized on the oxide surface using an expoxysilane crosslinker. Chips were activated with 1:1 H_2O_2:H_2SO_4 solution for 15 min, rinsed with copious amounts of DI water, dried under high purity N_2 flow, and then transferred into a glove box purged with nitrogen for protection from humidity. Next, the activated chips were immersed in a 2.5% solution of (3-glycidoxypropyl)trimethoxysilane in anhydrous toluene, and were allowed to react at room temperature for 24 hours. Then chips were rinsed with toluene and methanol to remove excess of silane not covalently bound to the surface, placed in an oven at 120 °C for 30 min. We have observed that this coating retains functionality and reactivity at least a week after the procedure. 10 μM lysine modified PNA molecules were suspended in a 150 mM sodium phosphate buffer (pH 8.5) and were attached on the surface by spotting 5 μL of the solution on the chip and incubating in a high humidity chamber set at 42 °C for about 2 hours. The chip was then immersed in a pre-hybridization buffer, consisting of BSA (Bovine Serum Albumin) 1% w/w in 3x SSC (Saline Sodium Citrate) buffer for about one hour at room temperature to minimize the non-specific binding of species in further steps. Chips were rinsed with DI water and dried under N_2 flow. PNA immobilization was confirmed by fluorescence imaging and subsequently chips were immersed in a solution of 10 μM of LNA6-BHQ suspended in a 4xSSC solution. Chips were then allowed to incubate overnight at 55 °C. The chips were then rinsed with DI and dried with N_2. After incubation the attachment was confirmed by the lack of fluorescence due to the fluorescence quenching effect of BHQ. The chips containing the devices and the blank oxide chips were prepared using this procedure.

The localized exchange reaction was performed by applying 12 V_{rms} for heating with 10 μM LNA8 in 10^{-4} × TBE buffer for 20 min. The device was imaged before and after the application of heat.

Results and Discussion

FET Devices as Sensors

The electrical configuration for both sensing and heating are shown in Figure 2a. For sensing, the back gate (V_{BG}) and fluid gate (V_{FG}) biases are swept to modulate the carrier

concentration in the channel while the source-drain current (I_{DS}) is measured with a constant source-drain voltage (V_{DS}). As changes in the charge occur at the surface of the devices (due to changes in pH or the binding of biomolecular analytes), the surface potential at the fluid/gate dielectric interface changes, modulating the carrier concentration and thus the source-drain current. For heating, the source and drain nodes of the device to be heated are shorted, and an AC bias is applied between this node and the back gate with the fluid gate held floating.

We first demonstrated normal transistor operation of the devices in a dry state. The source-drain current was measured as the back gate voltage was swept (Figure 2b). The devices exhibited subthreshold slopes of around 300 mV/decade, with threshold voltages around −2 V. In addition, the leakage current consistently stayed below 1 nA, showing that the device was stable and functional. Next, 10 mM solutions of sodium phosphate buffers at two different pH values, 5.4 and 8.1, were placed over the devices, and the double gate characteristics were measured (Figure 2c). Both the fluid gate and back gate biases could be seen to control the channel concentration and thus the source-drain current. In addition, when changing the pH of the solution from 5.4 to 8.1, increases in current were seen for nearly all biases, which is expected for p-type devices biased in accumulation. However, as has been explored previously[27], certain biasing regions lend themselves for optimized sensitivity, such as the region circled in the figure, where current increases of approximately two orders of magnitude could be observed. The devices were thus seen to be sensitive to changes in charge at the surface in fluid, and with further optimization could be used as sensors of pH, DNA, or protein.

Determination of the Spatial Resolution of Heating

The heating technique, mechanism, and the measurement of the temperature at the surface was described in detail previously[17]. Briefly, we introduced a technique to locally heat fluid within 2 nm of an oxide surface by using radio-frequency Joule heating of mobile ions in the Debye layer close to the device surfaces. We also demonstrated a measurement technique to extract the temperature at the surface of the devices, using the temperature modulated decay rate of the observed fluorescence while exposing the devices to high intensity light. Using this technique, we were able to correlate applied AC biases with the achievable temperature on the surface. Furthermore, we demonstrated several control experiments further validating that the observed fluorescence behavior was a result of changes in temperature, as opposed to other mechanisms that could modulate fluorescence.

To further establish the physical basis of the heating at the sensor surface and determine the spatial resolution of the heating technique, we measured the heating profile directly over the devices. Texas Red labeled DNA was attached to the surface of the sensors (see Materials and Methods). After the application of heat to the device, partial removal of the DNA oligomers was observed, resulting in a decrease of fluorescence in areas where the temperature was the highest (Figure 3b,c). Temperature-mediated removal of self-assembled monolayers (SAMs) has been observed previously; earlier work has reported that SAMs on oxidized silicon substrates and glass slides are unstable over 80°C [28]. This comparison is not intended as an approximation of the temperature on the surface, but rather as an indication that these films will indeed become unstable at higher temperatures. This work used thiol modified DNA oligomers to attach to the SAMs as opposed to the amine modified DNA used in this work, but the attachment of the SAMs to the oxidized silicon substrates employs the same silane chemistry.

We then explored the heating of buffer solution due to the applied AC field through simulations. A stack similar to the TEM cross section in Figure 3a was used. In general, the electric field should be calculated by solving the Poisson equation exactly; i.e.,

$\nabla \cdot (\varepsilon \nabla \Phi) = Q_s + \rho_{ion}$, where ε is the dielectric constant, is Φ the total potential, Q_s is the surface charge-density which consists of the ionized silanol (Si-OH) bonds and any target-receptor pair on the surface, and ρ_{ion} is the ion concentration of the buffer solution. Due to the presence of surface charge Q_s, the counter-ion density decays exponentially to its bulk value. The potential $\Phi = \Phi_s + \Phi_{AC}$ is the sum of the potential created by the surface charge and the potential due to AC voltage. Due to the relatively high frequency (10 MHz) used, negligible electrostatic screening occurs in the buffer solution. Therefore, Poisson's equation may be solved by solving two partial differential equations ($\nabla \cdot (\varepsilon \nabla \Phi_{AC}) = 0$, and $\nabla \cdot (\varepsilon \nabla \Phi_s) = Q_s + \rho_{ion}$, in two dimensions for the sensing region. As expected, the maximum electric field intensity ($E_{AC} = -\nabla \Phi_{AC}$) occurs near the edges of active silicon region due to the fringing effects (Figure 3d), and hence will result in higher temperature at the edges. The heat transport in the system was modeled using the thermal diffusion equation $\nabla \cdot (\kappa \nabla T) = \sigma(\rho) E^2/2 \approx \sigma(\rho_{ion}) E^2/2$, where κ is the thermal conductivity, T the temperature, σ the electrical conductivity of the medium ($\sigma = \omega \varepsilon''$), and E the local electric field obtained by numerical solution of Poisson's equation. Here we assume that dielectric heating of counter-ions at nanoscale regime also follows the classical $P = \sigma E^2/2$ dependence, where P is the power dissipated in an AC field. $E \approx E_{AC}$ because the magnitude of the AC field (~20–30V_{RMS}) is significantly greater compared to the potential due to the surface species (~0.25 V). Due to the presence of surface charge, the counter-ion density and hence the local conductivity (σ) near the sensor surface is much higher than in the bulk buffer. Due to the high fringing electric fields, maximum heat generation occurs close to the edges of the sensing region (Fig. 3e, f). These results compare well to the experimental observations shown in Figure 3b and 3c. From these results, we can conclude that the spatial spread in the heat profile is less than 1 μm in the lateral direction (from both experimental observations and simulation results) and less than 3 μm in the vertical direction (from the simulation results). Thus, a spatial resolution in the heat using this technique is easily below a few microns in all directions.

We also used numerical simulations to indicate that dielectric heating of the counter-ions is indeed the dominant mechanism. On applying an AC bias, heat generation could occur due to a combination of the following mechanisms: (i) dielectric loss in SiO_2 (the BOX and the oxide which covers Silicon active area), (ii) dielectric loss in buffer solution, especially due to the counter-ions. The total amount of power (P) converted into thermal energy in SiO_2 is given by $P = 1/2\, \sigma |E|^2$, where consider $\sigma = \varepsilon'' \omega$. We use $\varepsilon'' = 3.9$ for SiO_2 and σ for counter-ions is taken to be proportional to the counter-ion density, the multiplicative factor is used as a fitting parameter to scale simulation results to the experimental range. Supplementary Figure 1a indicates that the contribution of dielectric loss in SiO_2 is negligible. Thus, our simulations and experimental results clearly indicate that counter-ion heating is the dominant mechanism.

As the device width is scaled down further, the temperature uniformity and the average temperature of the fluid on the device for a given voltage also increases (Supplementary Figure 1b) as the region influenced by the fringing fields forms a larger portion of the device cross section. Aggressive scaling in size reduces the volume over which heat generation can occur and thermal diffusion limits achievable temperatures for given voltages (for widths less significantly less than 1 μm). However, a biological relevant temperature range of 30–70 °C should be possible for devices with sub micron widths. Scaling down the devices to the nanoscale should only improve the spatial resolution and uniformity of the heating technique.

Heat Mediated Exchange Reaction

To demonstrate the utility of the heating technique for bio-chemical applications, we have carried out a temperature-mediated exchange reaction as a model reaction on the surface of transistors (Fig. 4a). The scheme involves selectively exchanging a higher affinity molecule (8-mer LNA) with a lower affinity molecule (6-mer LNA) already bound to a surface capture probe (PNA) by enhancing the local reaction rate due to the local temperature. Table 1 shows the molecules used in our studies. We monitor the reaction by modifying the PNA probe with a fluorophore, and modifying the 6-mer LNA with a black hole quencher (BHQ). The decrease in the fluorescence intensity indicates the presence of the 6-mer LNA-PNA duplex due to the quenching effect. The recovery of the fluorescence indicates the presence of the 8-mer LNA-PNA duplex. The model exchange reaction was studied in solution phase before being applied to the surfaces. Dynamics of the FAM-PNA8 (10 μM) and the LNA6-BHQ duplex was studied by obtaining the melting-annealing curves from 20 °C to 94 °C (Fig. 4b) by monitoring the relative fluorescence intensity of the FAM-PNA8 (CARY Eclipse Fluorescence Spectrophotometer). The melting temperature was observed to be above 90 °C. The duplex was then heated in the presence of the LNA8. The exchange reaction was indicated by an increase in fluorescence at a relatively lower temperature than observed in the melting curve. Next, the exchange reaction was studied on a blank surface using bare oxide chips and a warm stage to control the surface temperature in the presence of the 10 μM LNA8 in 10^{-4} × TBE buffer. A fluorescence image was obtained at each temperature point, and the intensity was quantified as a function of the surface temperature (Fig. 4c). Similar to the data obtained in bulk solution, an increase in the overall intensity was observed with increasing temperature, indicating the execution of the exchange reaction on the surface. The fluorescence intensity did not recover to the intensity levels observed with the immobilized PNA before the hybridization of the LNA6-BHQ. We attribute the partial recovery of the fluorescence intensity to two factors: partial fluorescence quenching effect of the 8-mer LNA and increased photo-bleaching effects due to the high magnification objectives used.

The spatially localized reaction on the surface of a device was carried out by covalently attaching the lysine-modified PNA molecule (FAM-PNA8) and subsequently incubating with the 6-mer LNA (LNA6-BHQ) to form a duplex on the surface, resulting in decreased fluorescence compared to the PNA alone. With the application of 50 °C on the device (20 μm) for 20 minutes in the presence of the buffer solution containing 8mer LNA (LNA8), the heat-mediated exchange reaction took place on the devices resulting in a net increase in the fluorescence intensity on the device (Fig. 4d, e) without significantly affecting adjacent devices that were not heated. These experiments show that the devices can indeed be used to carry out localized biochemical reactions via the precise application of heat. Any chemical reaction that is catalyzed by increased temperature could potentially be performed in a similar fashion, confined only around the device of interest. The observed difference between the bulk behavior shown in Figure 4b (~250% increase) and that observed on the surface in Figure 4e (~60 %) could be due to the difference between the molecules present in solution and the molecules immobilized on a surface. Due to possible steric hindrance and conformational issues for surface immobilized molecules, the efficacy of reactions on a surface is expected to be different when compared to molecules free in solution. In addition, the bleaching effects of molecules immobilized on a surface could also be different than for molecules in solution.

Desorption and Refunctionalization for Selective Functionalization

The heating technique can also be utilized for carrying out reactions at superheated temperatures by applying higher voltages. As one potential application of superheating, we demonstrate the regeneration of the surface of the sensor by decomposing the species

attached on the surface via electrically addressable heat to the target device (Fig. 5a, b). By attaching both the probe and the complementary target on the surface, we studied the removal of the molecules from the surface. Removal of the full duplex, rather than only the target molecule indicated the decomposition of the molecules versus a denaturing event (Supplementary Figure 2a, b). The heat-mediated desorption of the molecules can also be used to perform selective functionalization of surfaces, which is very important for the realization of dense arrays of nano-biosensors. Attachment of two distinct DNA probes was demonstrated on adjacent devices by decomposing the species attached on the surface via electrically addressable heat to the target device, followed by repeating the molecule attachment protocol with a distinct probe molecule (Fig. 5c, d). Quantification of the change in fluorescence intensity showed a nearly complete removal of the first probe from initial functionalization to desorption and an increase in the fluorescence of the second probe from desorption to refunctionalization (Fig. 5e). Negligible changes were observed for an adjacent non-heated device. The selectivity of the attachment to the heated device suggests that the fluorescence intensity decrease after the heating is due to the complete removal of previously immobilized molecules from the heated devices. Further, refunctionalization experiments with the omission of the initial step of the functionalization process did not result with the immobilization of the new probe. Two sets of chips (Set A and Set B) were functionalized and desorbed, following an identical procedure to that outlined in the manuscript. The chips were first functionalized with a linear probe sequence D modified with a HEX fluorophore. Later, one device on the chip was heated to remove the previously immobilized probe, and the device was refunctionalized with linear probe sequence C modified with a FITC fluorophore. The refunctionalization of chips in Set A and Set B was carried out identically, with the exception of an omission of the 3% 3-aminopropyltrimethoxysilane in the silanization buffer for Set B. The results are shown in Supplementary Figure 2c. The figure demonstrates the refunctionalization of Set A with the FITC labeled probes, while Set B registered no increase in the fluorescence level (some red fluorescence is observed in the heated device, and some green intensity is registered in the non-heated device as a result of bleed through of fluorescence through the filters). These experiments suggest that the surface is available for silanization after heating, since all the chemistry steps, including the silanization, are needed to re-functionalize the surface of the devices.

This technique can be used for fine patterning of different probe molecules with high spatial resolution. In final applications, a technique such as this would need to be integrated with a rougher patterning technique, such as ink jet spotting of distinct analytes, which has a spatial resolution on the order of 50 μm with state-of-the-art techniques. With further scale down of the devices, the spatial resolution can be improved down to the nanoscale as per our simulations, eventually allowing for the ultra-dense patterning of probe analytes for dense sensors target at many distinct analytes simultaneously.

Conclusion

Our results indicate a high potential for wide ranging applications and high amenability of these FET hybrid sensor-heaters for further scaling down both the dimension of and the separation between devices, and increasing the spatial and temporal resolution of the technique. The current devices were shown to exhibit normal transistor behavior and to be sensitive to changes in pH. Furthermore, a heating spatial resolution of less than 3 μm was demonstrated in all directions, though this can be dramatically reduced as per our simulations. The devices were used to show proofs of concepts of the heating technique for two applications – a localized biochemical exchange reaction and the patterning of distinct probe molecules on the same chip. These field effect sensors with localized heating capability can be used to develop novel tools to be used in lab-on-a-chip systems such as

highly integrated PCR systems, active sensor surfaces that can be regenerated, creating localized heat-mediated incisions on single cells, and dense sensor arrays for the multiplexed and label free detection of biomolecules.

Supplementary Material

Refer to Web version on PubMed Central for supplementary material.

Acknowledgments

We acknowledge the use of Micro and Nanotechnology Laboratory at UIUC for device fabrication, the Birck Nanotechnology Center at Purdue for initial device fabrication for equipment maintenance, UIC NCF staff for assistance with PECVD deposition, and S. Iqbal for providing some of the DNA sequences. We are grateful to T. Sands, D. Peroulis, D. Cahill, and W. P. King for helpful suggestions and discussions. This work was initially funded by NIH (R21-EB006308), NSF (ECS 0554990), and a seed grant from the Indiana Elks administered through the Purdue University Cancer Center, and now from NIH (R01CA120003).

References

1. Schaller RR. Ieee Spectrum. 1997; 34:52–59.
2. Bergveld P. Sensor Actuat B-Chem. 2003; 88:1–20.
3. Drmanac S, Kita D, Labat I, Hauser B, Schmidt C, Burczak JD, Drmanac R. Nat Biotechnol. 1998; 16:54–58. [PubMed: 9447594]
4. Zheng GF, Patolsky F, Cui Y, Wang WU, Lieber CM. Nat Biotechnol. 2005; 23:1294–1301. [PubMed: 16170313]
5. Kopp MU, de Mello AJ, Manz A. Science. 1998; 280:1046–1048. [PubMed: 9582111]
6. Huber DL, Manginell RP, Samara MA, Kim BI, Bunker BC. Science. 2003; 301:352–354. [PubMed: 12869757]
7. Waters LC, Jacobson SC, Kroutchinina N, Khandurina J, Foote RS, Ramsey JM. Anal Chem. 1998; 70:158–162. [PubMed: 9463271]
8. Park I, Li ZY, Pisano AP, Williams RS. Nano Lett. 2007; 7:3106–3111. [PubMed: 17894518]
9. Lee CY, Lee GB, Lin JL, Huang FC, Liao CS. J Micromech Microeng. 2005; 15:1215–1223.
10. Maltezos G, Johnston M, Scherer A. Appl Phys Lett. 2005; 87
11. Liu P, Seo TS, Beyor N, Shin KJ, Scherer JR, Mathies RA. Anal Chem. 2007; 79:1881–1889. [PubMed: 17269794]
12. Bengtsson NE, Ohlsson T. P Ieee. 1974; 62:44–55.
13. Bykov YV, Rybakov KI, Semenov VE. J Phys D Appl Phys. 2001; 34:R55–R75.
14. Fermer C, Nilsson P, Larhed M. Eur J Pharm Sci. 2003; 18:129–132. [PubMed: 12594005]
15. Goodwin DC, Lee SB. Biotechniques. 1993; 15:438. [PubMed: 8217156]
16. Shah JJ, Sundaresan SG, Geist J, Reyes DR, Booth JC, Rao MV, Gaitan M. J Micromech Microeng. 2007; 17:2224–2230.
17. Elibol OH, Reddy B, Nair PR, Dorvel B, Butler F, Ahsan ZS, Bergstrom DE, Alam MA, Bashir R. Lab Chip. 2009; 9:2789–2795. [PubMed: 19967115]
18. Fodor SPA, Read JL, Pirrung MC, Stryer L, Lu AT, Solas D. Science. 1991; 251:767–773. [PubMed: 1990438]
19. Bhatia SK, Hickman JJ, Ligler FS. J Am Chem Soc. 1992; 114:4432–4433.
20. Blawas AS, Reichert WM. Biomaterials. 1998; 19:595–609. [PubMed: 9663732]
21. Lee KB, Park SJ, Mirkin CA, Smith JC, Mrksich M. Science. 2002; 295:1702–1705. [PubMed: 11834780]
22. Kane RS, Takayama S, Ostuni E, Ingber DE, Whitesides GM. Biomaterials. 1999; 20:2363–2376. [PubMed: 10614942]
23. MacBeath G, Schreiber SL. Science. 2000; 289:1760–1763. [PubMed: 10976071]

24. Bunimovich YL, Ge GL, Beverly KC, Ries RS, Hood L, Heath JR. Langmuir. 2004; 20:10630–10638. [PubMed: 15544395]
25. Curreli M, Li C, Sun YH, Lei B, Gundersen MA, Thompson ME, Zhou CW. J Am Chem Soc. 2005; 127:6922–6923. [PubMed: 15884914]
26. Stern E, Klemic JF, Routenberg DA, Wyrembak PN, Turner-Evans DB, Hamilton AD, LaVan DA, Fahmy TM, Reed MA. Nature. 2007; 445:519–522. [PubMed: 17268465]
27. Elibol OH, Reddy B, Bashir R. Appl Phys Lett. 2008; 92
28. Chrisey LA, Lee GU, OFerrall CE. Nucleic Acids Res. 1996; 24:3031–3039. [PubMed: 8760890]

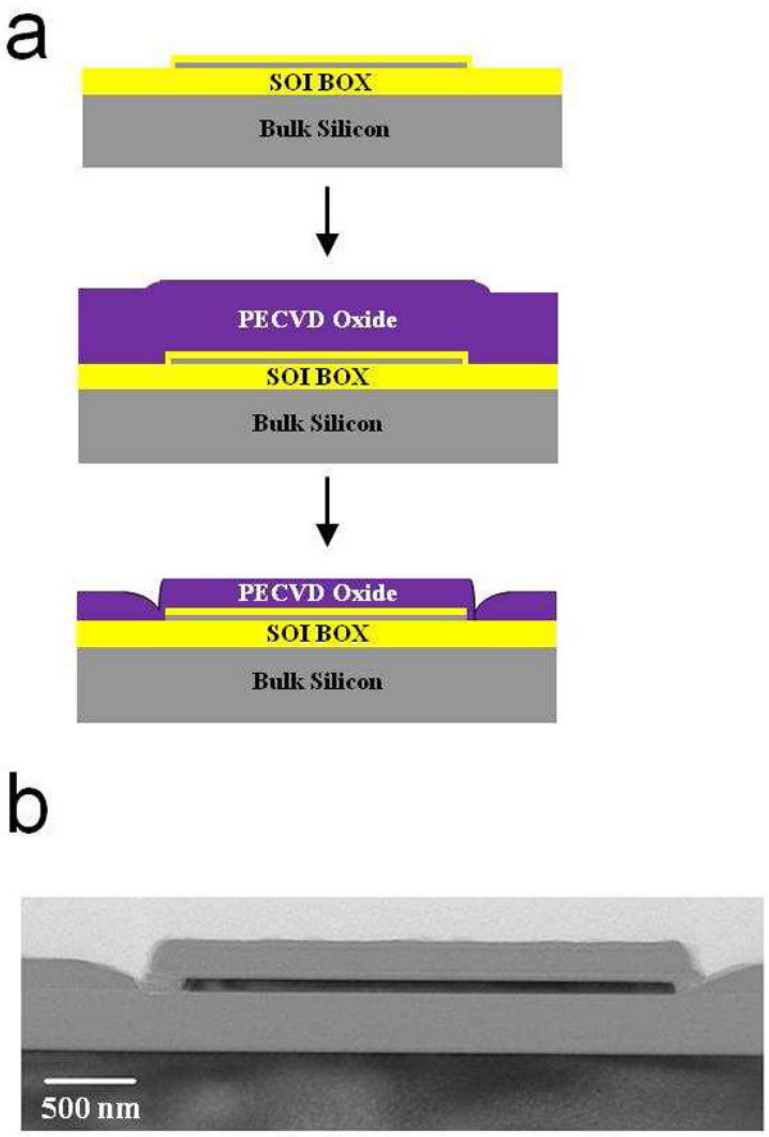

Figure 1.

Illustration of the device structures. **a**, Key steps in the fabrication process, including the etchback step to expose the surface of the devices to the fluid. **b**, SEM micrograph cross section of a typical nanoplate sensor-heater.

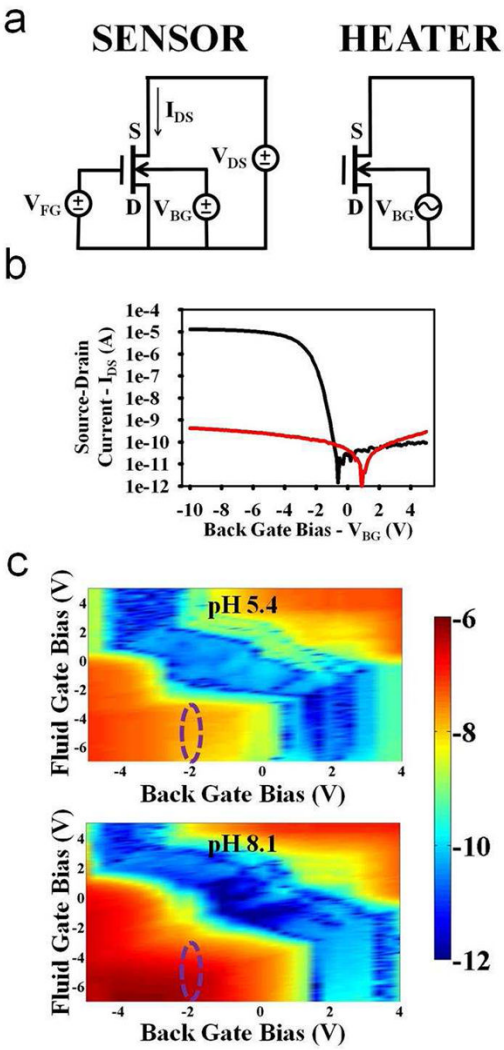

Figure 2.

Electrical sensing results. **a**, Electrical configurations for the use of the devices as electrical label-free sensors (left) and as localized heaters (right). **b**, Transfer characteristics of the devices while operating as sensors. Source-drain current is shown as a function of applied back gate voltage (black). Also plotted in red is the gate leakage current. **c**, Two dimensional plots showing the source-drain current as a color plot as a function of both the applied back gate and fluid gate biases. Normal transistor operation is seen using both of the gates. When the pH is changed from 5.4 to 8.1, substantial increases in currents are observed, especially in regions of optimal biasing, such as the one circled in purple.

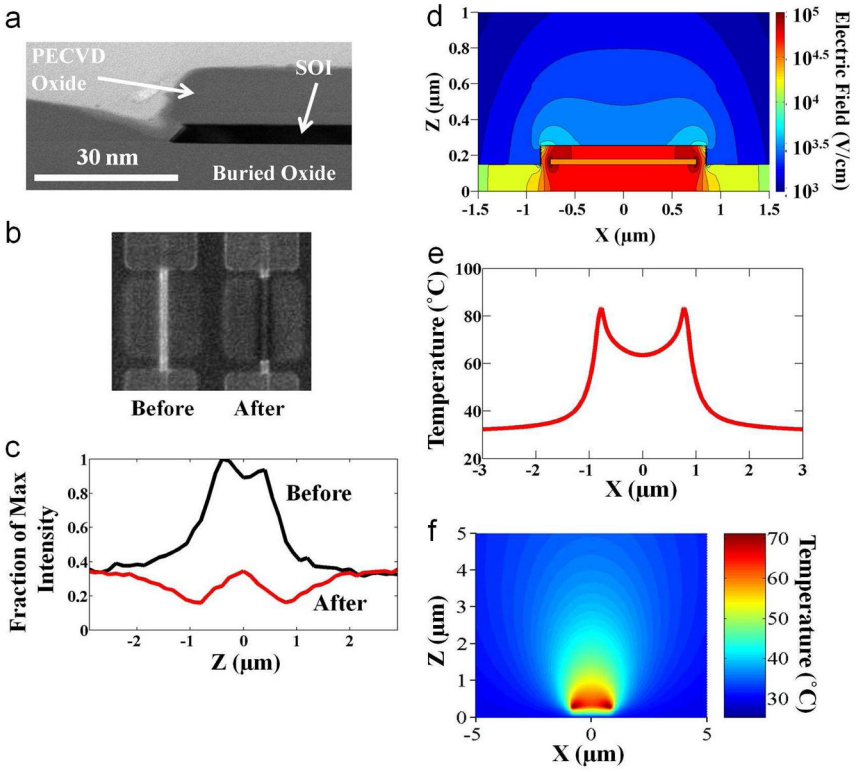

Figure 3.

Investigation of the heating mechanism and determination of the spatial resolution of the technique. **a**, Zoomed in cross sectional transmission electron micrograph of the device types for experimental and simulation results after the final fabrication step. **b**, Fluorescent images demonstrating the experimental heating desorption profile. A picture of the device to be heated prior to the application of voltage is shown on the left. To the right is a fluorescent picture acquired after the device was heated to an intermediary voltage to demonstrate the heating profile. **c**, Quantification of the fluorescent images in part b demonstrating similar trends. **d**, Simulated electric field strength around the device showing that higher fields are concentrated around the sidewalls of the device in fluid. **e**, One-dimensional simulated temperature distribution depicting the localized nature of AC heating technique as a function of lateral position through the device cross section. **f**, Two-dimensional simulated temperature distribution showing that the spread is less than ~3 μm in both the horizontal and vertical directions.

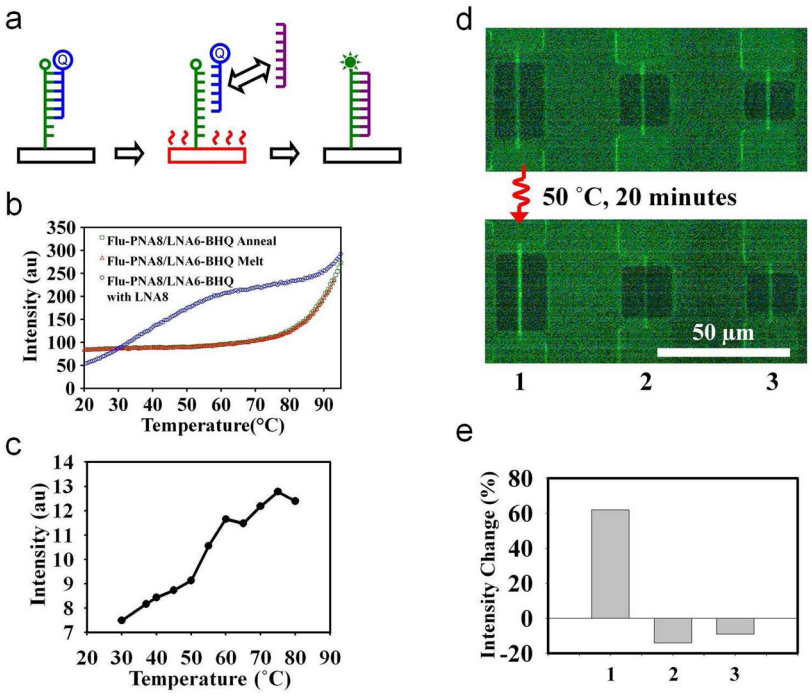

Figure 4.

Heat mediated localized exchange reaction. **a**, Schematic demonstrating the concept of the exchange reaction. **b**, Fluorescence intensity as a function of temperature at different conditions. Melting of the PNA-LNA duplex happens at relatively high temperatures (red and green) when compared to competing LNA molecules (blue curve). The presence of the LNA thus allows for the recovery of the fluorescence at relatively low temperatures. **c**, Exchange reaction studies on a blank silicon-dioxide chip by externally heating to known temperatures. **d**, Fluorescence images showing the experimental results. Top image is taken before the experiment. Below is the image after exposing the chip to the higher affinity molecules while simultaneously heating device 1 (left most, shown with a curly red line, device 5 µm in length) for 20 minutes. **e**, Average fluorescence intensity increase for each device before and after the experiment. The slight decrease in the fluorescence intensity for the non-heated devices is due to photo-bleaching.

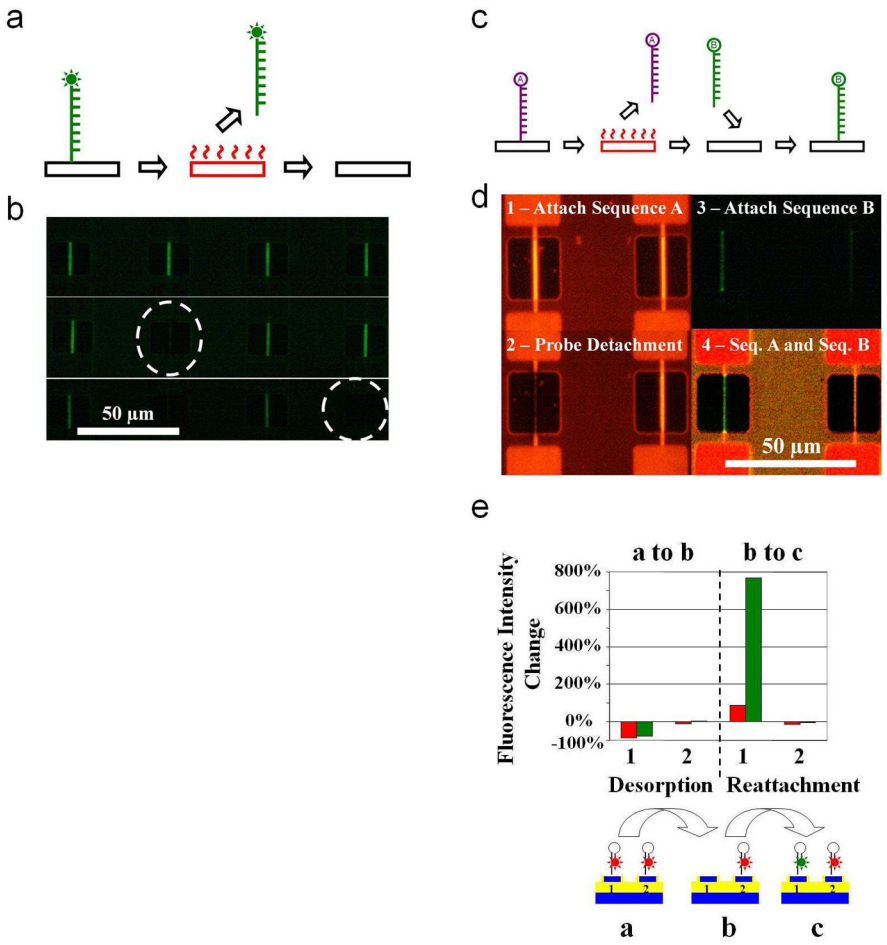

Figure 5.

Localized decomposition of immobilized molecules, and subsequent refunctionalization of the surfaces. **a**, Schematic summarizing the procedure for the heat mediated localized decomposition of the molecular layer. Device is represented with a black rectangle, and red indicates voltage applied to the device. After the immobilization of the appropriate functional layer on surface, the desired surface is heated by the application of voltage for the decomposition of the molecule. **b**, Fluorescent images showing the electrically addressable decomposition of the functional layer. The top image is taken before the experiment. Consecutive images (middle and bottom) are taken after heating the device encircled with dashed white lines. **c**, Similar to part a, but summarizing the procedure for the heat mediated localized functionalization of a device. A device can be re-functionalized with a desired probe after the desorption of the previous molecule. **d**, Fluorescent images summarizing the selective functionalization procedure. Initially a fluorescently tagged (HEX Sequence A) is immobilized on all the devices (1). The immobilized probe is desorbed by heating the left device (2). After this step, the chip undergoes the immobilization procedure for a distinct probe molecule containing fluorescently modified Sequence B (3). The last image in the series was obtained using a triple filter spanning both wavelengths for the imaging of the fluorophores simultaneously, and demonstrates the final patterning of two distinct probe molecules on adjacent devices separated by 50 µm (4). **e**, Percent fluorescence intensity change using both the TRITC (red bars) and FITC (green bars) filters during each of the steps displayed in part d.

Table 1

Molecules Used in all Experiments

Sequence Description and Name	Sequence
DNA Molecular Beacon Probe (Probe 1)	5′-FITC-C6-CCAACGGTTGGTGTGTGGTTGG-C6-DABCYL-Amine-3′
DNA Target for Molecular Beacon Probe (Target 1)	5′-CCAACGGTTGGTGTGTG-C6-ROX-3′
DNA Hairpin loop Probe Sequence A (Sequence A)	5′–HEX-C6-CCAACGGACGTCGAATGGTTGG-C6–Amine-3′
DNA Hairpin loop Probe Sequence B (Sequence B)	5′-FITC-C6-CCAACGGTTGGTGTGTGGTTGG–C6-Amine-3′
DNA Linear Probe Sequence C (Sequence C)	5′-FITC-C6-CCAACGGTTGGTGTGTG-C6-Aniine-3′
DNA Linear Probe Sequence D (Sequence D)	5′-HEX-C6-CCAACGGACGTCGAATG–C6-Amine 3′
PNA 8-mer	N-FAM-OO-GCATCGTA-Lysine-C
LNA 6-mer	5′-CGATGC-BHQ1-3′
LNA 8-mer	5′-TACGATGC-3′